

E-ISSN: 2664-7583 P-ISSN: 2664-7575 Impact Factor (RJIF): 8.12 IJOS 2025; 7(2): 217-224 © 2025 IJPA www.physicsjournal.in

Received: 07-09-2025 Accepted: 09-10-2025

#### Dr. KSS Raja Sekhar

Principal, Government Junior College, Yeleswaram, Kakinada District, Andhra Pradesh, India

## The solar and stellar activity

### KSS Raja Sekhar

**DOI:** <a href="https://www.doi.org/10.33545/26647575.2025.v7.i2c.197">https://www.doi.org/10.33545/26647575.2025.v7.i2c.197</a>

#### Abstract

This chapter presents a comprehensive examination of magnetic activity in the Sun and other stars, with particular emphasis on its physical origin, observational manifestations, and implications for exoplanetary studies. The discussion begins with an overview of the Sun's magnetic activity, tracing its evolution from the photosphere through the outer atmospheric layers. Key features, including sunspots, faculae, and chromospheric structures, are described in the context of their temporal variability, commonly referred to as the solar activity cycle. The persistence of these phenomena throughout the solar lifetime is attributed to the operation of a magnetic dynamo, maintained by differential rotation and convective flows. Extending these concepts to stellar contexts, the chapter explores the diagnostics employed to monitor and quantify stellar magnetic activity, with particular attention to spectropolarimetry as a primary observational technique for characterising stellar magnetic fields. The synthesis of empirical results and theoretical modelling is then presented across a range of spectral types, providing insights into the diversity of stellar activity patterns. Finally, the chapter reviews current methodologies for detecting stellar activity cycles and highlights the multi-wavelength approaches that underpin contemporary investigations in this domain.

**Keywords:** Solar magnetic activity, stellar magnetic fields, magnetic dynamo, Spectropolarimetry, stellar activity cycles sunspots, exoplanetary environments

#### Introduction

The most widely employed techniques for exoplanet detection are indirect, relying on the influence of planets on their host starlight over time rather than on direct measurements of planetary properties. A natural implication of this dependence is that a deeper understanding of stellar properties directly enhances the robustness of exoplanet detection and characterisation. In this framework, stellar activity is of central importance. It encompasses the ensemble of dynamo-driven magnetic phenomena manifesting on stellar surfaces and extending outward into their atmospheres. Disentangling planetary signals from stellar-induced variability requires precise knowledge of surface flux inhomogeneities and their temporal behaviour.

The Sun provides the nearest and most detailed laboratory for investigating stellar magnetic activity. Its magnetism arises from the solar dynamo, a process governed by the coupling between differential rotation and convective motions in the solar interior. This mechanism sustains the solar magnetic field, which exhibits cyclic modulation, most prominently the ~11-year sunspot cycle characterised by variations in sunspot number and spatial distribution. While extensively studied, the solar dynamo remains an area of active investigation, with state-of-the-art numerical models striving to reproduce observed magnetic cycles. Beyond the photosphere, magnetic influences extend into the corona, where they drive energetic processes such as solar flares and coronal mass ejections. These phenomena modulate the solar wind and space weather, thereby shaping planetary environments, including the terrestrial magnetosphere.

Analogous processes are observed in other stars, where manifestations of magnetic activity include star spots, high-energy flares, and long-term activity cycles. The characteristics of stellar activity vary systematically with fundamental stellar parameters, including mass, rotation, and internal structure. Moreover, stellar magnetic fields regulate high-energy radiation and stellar winds, both of which exert profound influence on the circumstellar environment. These interactions play a pivotal role in the evolution of exoplanetary atmospheres and shape planetary habitability conditions over long timescales. Accordingly, comparative studies of stellar activity across spectral types provide the foundation for a comprehensive framework of stellar magnetism and its role in planetary system evolution.

Corresponding Author: Dr. KSS Raja Sekhar Principal, Government Junior College, Yeleswaram, Kakinada District, Andhra Pradesh, India

#### 1. Solar magnetic activity

Signatures of solar and stellar activity at optical and near-infrared wavelengths originate from the photosphere and chromosphere. The photosphere is the lowest layer of the stellar atmosphere and, in the case of the Sun, has an effective temperature of 5772 K. Above this layer lies the chromosphere, which shows a temperature minimum at about 500 km above the  $\tau500=1$  surface, followed by a rapid rise to several tens of thousands of Kelvin around 2000 km. The chromosphere is highly heterogeneous, with a complex magnetic topology and transient features that evolve on timescales of minutes.

Advances in solar observations with high spatial and temporal resolution have revealed a wide range of photospheric structures, including convective granules, dark sunspots, and bright faculae. Active regions originate from the emergence of magnetic flux tubes whose intense magnetic fields, on the order of kilo-Gauss, inhibit convection and modify local energy transport. Sunspots, with temperatures between 4000 K and 5000 K and magnetic field strengths between 1 and 4 kG, often form in clusters known as nests that display intricate structures and dynamics. Flux tube emergence also produces bright photospheric and chromospheric features, identified as faculae and plages, respectively, which are most visible near the solar limb. These regions are typically several hundred Kelvin hotter than the surrounding photosphere and persist from hours to days depending on whether they are isolated or grouped.

The periodic modulation of sunspot occurrence was first identified in the 19th century, revealing the 11-year Schwabe cycle. During cycle maxima, the number and size of sunspots increase, while minima are characterised by weak activity. On average, monthly sunspot numbers range from fewer than 20 at minimum to nearly 200 at maximum, though both amplitude and duration vary from cycle to cycle. At the start of a cycle, sunspots appear at mid-latitudes and progressively migrate toward the equator, a phenomenon described by Spörer's law and captured in the butterfly diagram. Irregularities in the solar cycle, including prolonged episodes of diminished activity such as the Maunder minimum, underscore its variability.

The discovery of the magnetic nature of sunspots and

subsequent identification of polarity reversals established the 22-year Hale cycle, comprising two consecutive sunspot cycles. During minima, the large-scale solar magnetic field is primarily dipolar, whereas maxima are marked by increasingly complex configurations involving quadrupolar and higher-order modes. The balance of energy between the poloidal and toroidal field components evolves throughout the cycle, while the geometry of the poloidal dipole oscillates between axisymmetric and non-axisymmetric states.

Above the chromosphere lies the narrow transition region, where temperatures rise sharply from about 50,000 K to nearly one million Kelvin. Beyond this extends the corona, a region of ionised plasma at temperatures of several million Kelvin that expands outward into interplanetary space as the solar wind. The unexpectedly high coronal temperatures, much greater than those of the underlying photosphere, pose the long-standing "coronal heating problem." Potential explanations include the dissipation of magnetohydrodynamic waves, small-scale magnetic reconnection, and turbulent processes. The corona becomes visible to the naked eye during total solar eclipses as a diffuse halo produced by Thomson scattering, and is routinely studied at radio and X-ray wavelengths.

The coronal spectrum is dominated by radiation from highly ionised plasma confined by magnetic fields. X-rays, spanning approximately 1–100 Å, arise predominantly in the corona, while extreme ultraviolet radiation between 100 and 912 Å originates both in the transition region and in the corona. Observations in these spectral bands provide critical diagnostics of coronal density, structure, and magnetic complexity. Moreover, X-ray and EUV emissions vary by an order of magnitude over the course of the solar cycle, reflecting their dependence on the magnetic dynamo.

High-energy radiation from solar and stellar coronae plays a fundamental role in shaping planetary atmospheres. X-rays penetrate deeper layers, while EUV radiation is absorbed higher in the atmosphere, leading to ionisation, dissociation, and heating processes that drive atmospheric escape. Over long timescales, these interactions influence the evolution of exoplanetary atmospheres and contribute to determining planetary habitability.

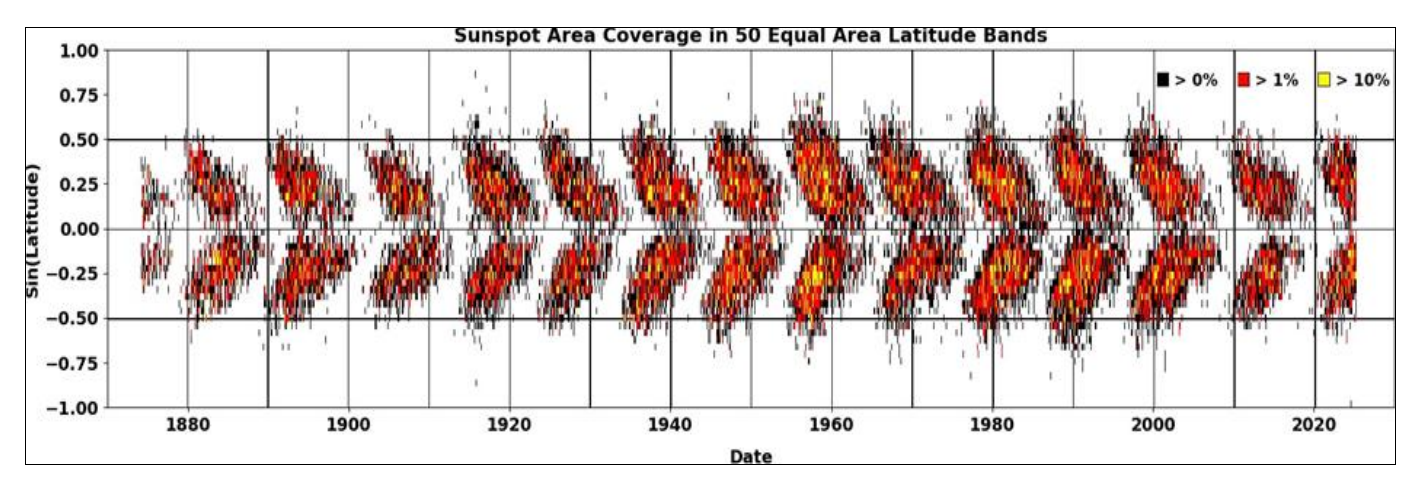


Fig 1: The butterfly diagram illustrates the distribution of sunspots and magnetic flux on the Sun and their change over time. The figure shows the sunspots area coverage as a function of latitude, for which it is possible to see the Sp¨orer law, that is the equatorward drift of the sunspot emergence through a magnetic cycle. Credit: Dr. D. Hathaway http://solarcyclescience.com/solarcycle.html.

#### 1.1 The solar dynamo theory

The Sun consists of a radiative core and a convective envelope, separated by the tachocline, a shear layer thought to store and amplify magnetic flux before its emergence as

surface spots. Solar magnetic field regeneration is explained by dynamo theory, where plasma motions convert kinetic energy into magnetic energy through the coupling of rotation and convection. The magnetohydrodynamical induction equation governs this process, combining induction and diffusion, with their balance quantified by the magnetic Reynolds number. A seed magnetic field, compliance with  $\nabla \cdot B = 0$ , and fluid dynamics from the Navier–Stokes equations are necessary to sustain the field against Ohmic decay.

Two main mechanisms are invoked: the  $\alpha\Omega$  dynamo, where differential rotation generates toroidal fields and turbulence regenerates poloidal fields, and the Babcock–Leighton mechanism, where tilted bipolar sunspot regions migrate poleward to restore the poloidal component. While both

frameworks reproduce aspects of solar magnetism, they fall short of explaining all observed features.

Numerical simulations highlight the role of the tachocline but also suggest self-organization within the convection zone. Recent models reproduce polarity reversals and oscillatory cycles, yet a unified dynamo theory remains incomplete. Future progress requires combining high-resolution solar observations with stellar magnetic cycle studies to constrain models across a wider parameter space.

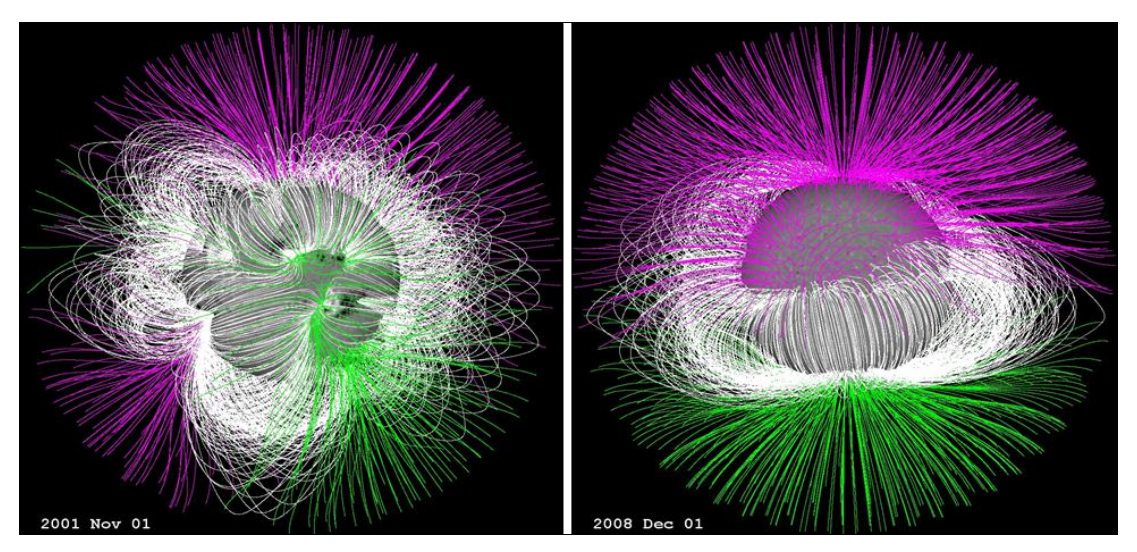


Fig 2: Potential Field Source Surface (PFSS) model of the Sun during cycle maximum and minimum. The images are built using the SolarSoft package from solar magnetograms collected by means of SOHO/MDI and SDO/HMI instruments, and the extrapolation is performed from the photosphere out to about 2.5 solar radii, which is where the source surface is located. The left image (November 2001) illustrates the magnetic field of the Sun at activity maximum (during cycle 23) and the right image (December 2008) illustrates the magnetic field at the activity minimum (and the start of cycle 24). Purple and green colours indicate open field lines of negative and positive polarity, while the white colour indicates closed field lines. The large-scale magnetic field has a simple, mostly dipolar configuration at activity minimum, and a complex one at activity maximum. Credit: NASA's Goddard Space Flight Center Scientific Visualization Studio/Bridgman and Duberstein.

# 2. Stellar magnetic activity 2.1 Starspots

Counting sunspots on the Sun provides a direct and reliable measure of solar activity due to the high spatial resolution available. Observations of other stars, which appear as unresolved point sources, require indirect approaches to evaluate activity. In these cases, the photometric variability of the star is monitored, as temporal modulations in the light curve are assumed to result from surface inhomogeneities. Complex light curves may reflect large-amplitude spot modulations or transits of co-rotating gas clouds. In some instances, modeling the light curve allows the reconstruction of starspot distributions. For stars known to host transiting exoplanets, variations in the transit light curve caused by the planet occulting dark spots can provide estimates of magnetic fields within the spots by relating their flux deficit to spot area and brightness.

Starspots also induce variability in spectroscopic and spectropolarimetric observations. A dark spot disrupts the balance of emitted flux between the approaching and receding hemispheres, producing distortions in spectral line profiles and apparent Doppler shifts that are modulated by stellar rotation. These distortions complicate the detection of exoplanets via radial velocity methods, as they can mimic or obscure planetary signals. Additionally, spots inhibit convective blueshift by reducing the contribution of rising hot plasma relative to cooler, darker regions, further affecting the observed spectral features.

Time-resolved monitoring of spectral line distortions enables

Doppler imaging, a tomographic inversion technique that reconstructs two-dimensional maps of stellar surface brightness. The longitudinal location of a spot is inferred from the timing of its spectral distortion, while the extent of the distortion across the line profile informs its latitudinal position. The resolution of the reconstructed map depends on the stellar rotational velocity, with higher rotation rates providing more reliable surface mapping. Complementary approaches using molecular line spectroscopy, such as the analysis of TiO absorption bands, allow the determination of starspot temperatures and surface filling factors. By combining spectra representing active and inactive photospheres, the spot contribution can be isolated, providing constraints on both temperature and area coverage.

Magnetic fields within starspots have been measured at different atmospheric depths, revealing that the complexity of magnetic structures varies with spectral type and atmospheric layer. Lower atmospheric layers of early-M dwarfs tend to exhibit simpler magnetic spots, while upper layers display more complex structures across spectral types. Some studies have found consistent field strengths across atomic and molecular indicators, highlighting the need for further investigation to fully understand magnetic structuring in stellar atmospheres.

Photometric indices derived from light curves, such as the rotationally segmented standard deviation, provide a global measure of stellar magnetic activity. Light curves are divided according to the stellar rotation period, and the standard deviation of each segment reflects the temporal evolution of

activity. The mean value over all segments represents the overall magnetic activity level of the star. Starspots persist over timescales ranging from a few days to several rotation cycles, with lifetimes and variability correlated to their size and the stellar spectral type. These observational techniques

collectively provide critical insights into stellar surface inhomogeneities and magnetic activity, which are essential for interpreting stellar variability and assessing the influence of stellar magnetism on exoplanet detection and characterization.

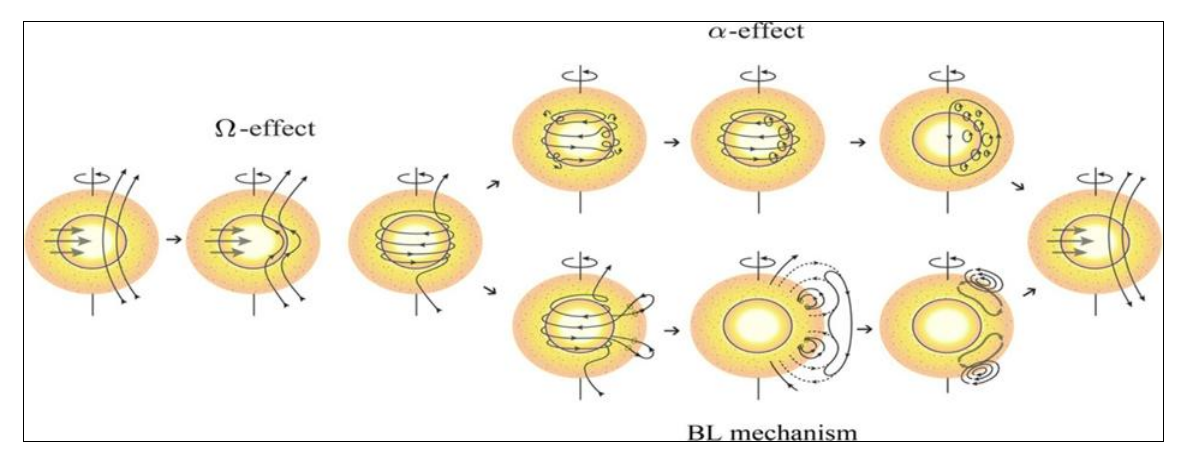


Fig 3: Mechanisms at the base for the solar dynamo model. The  $\Omega$ -effect transforms a poloidal field into a toroidal field via differential rotation. Restoring a poloidal field from a toroidal field is accomplished in two ways: the  $\alpha$ -effect sees cyclonic turbulence twisting toroidal field lines into small-scale poloidal fields which, on average, constitute a global poloidal field. The Babcock-Leighton (BL) mechanism sees the formation of bipolar regions on the surface; those close to equator diffuse and reconnect between hemispheres, whereas the remaining ones are transported towards the pole by meridional circulation and produce a large-scale poloidal field. Image credit: Sanchez *et al.* (2014) [28].

#### 2.2 Magnetic fields

Magnetic field measurements at the stellar photosphere rely mainly on the Zeeman effect (Zeeman, 1897), which occurs when atoms and molecules are subject to external magnetic fields. More details can be found in the lecture notes by Landstreet (2009a, b, c). The quantum energy levels split in a certain number of sub-levels depending on the total angular momentum quantum number J, with associated spectral lines, in absorption or emission. Considering a normal Zeeman triplet the amount of splitting (in nm) is expressed by the following formula in CGS unit system.

$$\Delta \lambda = \frac{e}{4\pi m_e c^2} \frac{\lambda^2}{g^0} \ \ \mbox{eff} \ B = 4.67 \cdot 10^{-12} \lambda^2 g \ \mbox{eff} \ B, \label{eq:delta}$$

With e the elementary charge, me the mass of the electron, c the speed of light, B the modulus of the magnetic field (in G), λ0 the central wavelength in the absence of the field (in nm) and geff the Land'e factor. The Land'e factor is a dimensionless number spanning between 0 and 3 and represents the sensitivity to the magnetic field of a particular line. It can be computed using a simple analytical formula in the case of L-S coupling. Besides the Zeeman effect, there are other quantum mechanical effects resulting in energy changes of atomic levels that reflect in changes of line profiles and polarisation properties. Depending on the magnetic field strength, there are indeed different regimes: for atomic lines, between 50 and 100 kG we have the Paschen-Back regime (weakly magnetised degenerate stars), whereas above 100 kG (magnetised white dwarfs) we have the quadratic Zeeman effect. For non-degenerate stars on the main sequence with fields up to 10 kG these effects are not observable, although in some cases the Paschen-Back effect can be observed.

#### 2.2.1 Magnetic field modulus and filling factor

Spectra in unpolarised light allow us to retrieve the total, unsigned stellar magnetic field. Assuming that the instrumental resolution is sufficient to distinguish the

Zeeman-split components of individual spectral lines, and that the splitting is larger than the intrinsic line width, the idea is to measure the wavelength separation between the components and solve the above equation for B.

When observing stars other than the Sun, further complications arise by the lack of spatial resolution, since observations convey only average information integrated over the stellar visible hemisphere, which is likely covered with inhomogeneities spanning a wide range of magnetic fields moduli and orientations. For unpolarised light, this means that we do not observe the Zeeman triplet clearly, but a more complicated and smeared pattern referred to as Zeeman broadening. This magnetic-induced broadening needs to be disen- tangled from non-magnetic line broadening (rotational, thermal, pressure, and instrumental). To disentangle Zeeman broadening, a possibility is to measure the width of individual atomic spectral lines formed under similar conditions, but with distinct magnetic sensitivities (Saar, 1988; Reiners, 2012) [29, 30]. Otherwise, one can use different sets of diatomic molecules depending on the star's spectral type, especially for those characterised by forests of molecular lines that reduce the number of unblended atomic lines to only a handful (Berdyugina et al., 2003; Afram and Berdyugina, 2015)[2]. An additional phenomenon affecting magnetically sensitive, saturated or damping-regime spectral lines is called magnetic intensification, which leads to the desaturation of these strong lines (Babcock, 1949; Basri et al., 1992) [11]. In practice, the Zeeman-induced splitting of an atomic line reduces the optical depth at its centre and increases the optical depth at the wings. As a result, the line centre is desaturated and its equivalent width is larger. As studied by Stift and Leone (2003), magnetic intensification correlates with the magnetic field strength, and it has a complicated and strong dependence on the Zeeman splitting pattern, opacity, and line strength which cannot be expressed analytically. By comparing equivalent widths of multiple lines with different magnetic sensitivities, it is possible to measure the magnetic field modulus (Basri and Marcy, 1994; Muirhead et al., 2020) [17, 31]. In addition, Muirhead et al. (2020) [31] recently showed the diagnostic

power of the so called curve-of-growth diagrams, in which the equivalent width of lines belonging to the same multiplet is plotted against their absorption cross-section parametrised by log(gf) (with f the oscillator strength and g a statistical weight). Depending on the trends on the curve-of-growth diagram, one can identify lines that belong to the saturated or the damping regime, hence susceptible to Zeeman intensification.

For M dwarfs in particular, spectrum synthesis modelling of the Ti I lines at 964.7-978.8 nm was adopted to perform extensive measurements (see Fig. 6), as they are excellent diagnostics for both Zeeman broadening and magnetic intensification. The output of these analyses is encapsulated in the disk-averaged magnetic flux Bf (measured in Gauss), where B is the modulus of the field and f is the filling factor in this context (not the oscillator strength), that is the portion of the stellar surface occupied by magnetic regions. Models postulate either a single value of B and f (Saar, 1988) [29] or a more elaborated multi-component, small-scale scenario (Johns-Krull *et al.*, 1999; Shulyak *et al.*, 2014) [32, 33], but in general these two quantities are degenerate. More precisely, a strong magnetic field covering a small portion of the star can be equivalent to a weaker field covering a larger portion of the star. This degeneracy is reduced when observations of strong magnetic fields are conducted at high-resolution, in near-infrared and encompassing high Land'e factor lines.

#### 2.2.2 Magnetic field vector

Owing to the Zeeman effect, circularly and linearly polarised spectra are sensitive to the magnetic field orien- tation, so they can be used to infer properties of the field geometry. In this case, the lack of spatial resolution translates into polarisation cancellation effects due to the contribution of areas with opposite field polarity, making the observations sensitive only to largest scales of the field. Therefore, repeated spectropolarimetric measurements are necessary to cover the rotation cycle of a star and eventually observe the magnetic field under different angles, namely a modulation of the polarity cancellation. This is a principal distinction with respect to Zeeman broadening analysis.

For active, cool main-sequence stars circular polarisation signatures are typically on the order of 10<sup>-3</sup> the level of unpolarised continuum and linear polarisation signatures are one order of magnitude smaller (Kochukhov et al., 2011; Lavail et al., 2018) [33, 26]. Observations of cool stars in linear polarisation mode are therefore limited to bright stars with strong surface magnetic fields. High-S/N observations are generally required to enable polarised Zeeman signatures to emerge from the noise and yield a reliable magnetic detection. In practice, for cool stars, this is achieved condensing the polarimetric information of the observed spectra into average line profiles using least-squares deconvolution (LSD Donati et al., 1997; Kochukhov et al., 2010) [33, 34]. Owing to the often unknown magnetic sensitivity for molecular lines, atomic absorption lines are used almost exclusively for this purpose. The output average profiles benefit from a S/N gain that scales with the square root of the number of lines used in LSD and varies between a factor of 10 and 30 for M and G dwarfs. Modern echelle spectropolarimeters are effective at combining high resolving power with large wavelength coverage for this purpose.

To reconstruct the large-scale magnetic field topology of a star, a tomographic technique called Zeeman- Doppler imaging (ZDI; Piskunov and Khokhlova 1983; Semel 1989; Donati and Brown 1997) [33, 34] is used. The concept is similar

to Doppler imaging (see Sect. 3.1), except that ZDI models rotationally modulated signatures of the magnetic field in circularly or linearly polarised light. The ZDI algorithm inverts a time series of polarised LSD profiles into a magnetic field map in an iterative fashion (for more information see Donati and Brown, 1997) [34]. More precisely, synthetic line profiles are compared and updated with respect to the observed

ones at each iteration, until convergence at a specific target  $\chi^2$  is reached. Such a problem is ill-posed,

meaning that infinite solutions could fit the observed data equally well, thus ZDI employs a regularisation scheme based on maximum entropy to choose a solution (Skilling and Bryan, 1984). The algorithm searches for the maximumentropy solution at a given  $\chi^2$  level, that is, the magnetic field configuration compatible with the data and with the lowest information content. An example of reconstructed magnetic field topology for two exoplanet host stars is given in Fig. 7. The vector magnetic field is modelled as the sum of a poloidal and a toroidal component, both expressed via spherical harmonics decomposition (Donati et al., 2006; Lehmann and Donati, 2022) [9, 27], which is in contrast with earlier attempts where the field was reconstructed independently on each surface element. Such formal approach ensures that the reconstructed field is divergence-free, and it is effective at describing the properties of the large-scale magnetic field geometry (e.g., poloidal or toroidal, and axisymmetric or nonaxisymmetric) and classify stars accordingly. The rotational velocity  $v_{eq} \sin(i)$  determines the maximum degree of the spherical harmonic expansion lmax in a proportional way, and therefore the amount of complexity we can image. In other words, given a complex field topology, a higher value of veq  $\sin$  (i) will translate in a higher achievable  $l_{max}$  and therefore a more structured description of the field. Moreover, faster rotation and thus rotational broadening implies that the Zeeman signatures are more separated in radial velocity space, ultimately limiting polarity cancellation. Although the method initially relies on the fact the field is steady and observed variations are only attributable to rotational modulation, limited temporal variability can be accounted for in the form of solar-like differential rotation, expressed as

$$\Omega(\theta) = \Omega_{eq} - d\Omega \sin^2(\theta),$$
 (3)

Where  $\theta$  is the colatitude,  $\Omega_{eq}=2\pi/P_{rot}$  is the rotational frequency at equator and  $d\Omega$  is the differential rotation rate in rad  $d^{-1}$ . We note that differential rotation is also implemented in Doppler imaging, meaning that it is possible to constrain such parameter also from a time series of unpolarised light observations.

## 2.3 Stellar dynamo models

Stars between mid-F and M3 spectral types are partly convective, featuring internal structures similar to the Sun with varying aspect ratios. Stars later than M3 are fully convective and lack a tachocline. Theoretical models place the transition between these regimes at approximately 0.35 solar masses, consistent with observations and used to explain features such as the Gaia magnitude gap. However, metallicity influences the depth of the convective envelope, and strong magnetic fields can suppress convection, effectively shifting this boundary to lower masses. Consequently, 0.35 solar masses should not be considered a sharp threshold. Understanding dynamo action across these different interior structures is essential to contextualize the

solar dynamo and investigate how magnetic field generation varies with stellar temperature, convective velocity, rotation rate, and Rossby number.

In partly convective stars, solar-like  $\alpha\Omega$  dynamos are generally invoked to explain magnetic field generation. The influence of stellar rotation and mass on the dynamo and resulting magnetic activity is complex and requires multidimensional numerical simulations to capture the excitation of various convective dynamo modes. Some studies extend mean-field solar dynamo models to other spectral types, while global three-dimensional magnetohydrodynamic simulations reproduce differential rotation and magnetic cycles in selected parameter regimes. Simulations of solar-like convective dynamos across different masses and rotation periods indicate long magnetic cycles for small Rossby numbers, whereas fast rotators often display irregular patterns. Fast rotators may also exhibit rapid evolution and localized polarity reversals.

Simulations of early-type, rapidly rotating M dwarfs show that a tachocline is not strictly necessary to generate strong, organized toroidal magnetic structures, although its presence can regularize magnetic cycles and support long-term variability. Fully convective stars, which lack a tachocline and exhibit nearly solid-body rotation, cannot sustain an  $\Omega$ -effectdriven dynamo. Early models invoked small-scale turbulent dynamos at the scale of plasma motions, while  $\alpha^{\scriptscriptstyle 2}$  dynamo models relying solely on cyclonic turbulence have also been explored. These models produce strong large-scale magnetic fields with significant axisymmetric components, but often fail to fully reproduce observations. Extensive research has focused on generating large-scale, axisymmetric dipoledominated fields, particularly under conditions of large density contrasts. Some studies reconcile observations of small- and large-scale magnetic fields, while mean-field dynamo models predict long-term evolution of field geometry without constraining global field strength. Targeted MHD simulations for stars such as Proxima Centauri successfully predict magnetic cycles consistent with observed photometric variations.

#### 3. Stellar cycles

Observing magnetic cycles in other stars than the Sun provides key constraints to dynamo theories, and in particular how fundamental stellar parameters, such as mass and rotation period, impact the internal dynamo processes (Jeffers *et al.*, 2023; Charbonneau and Sokoloff, 2023, for recent reviews). In the following, we summarise the observational techniques used to investigate the presence of stellar cycles and the main trends.

#### 3.1 Observational techniques

Long-term photometric time series provide direct evidence of stellar Schwabe cycles through surface inhomogeneities such as spots and faculae. Ground- and space-based observations spanning up to 40 years reveal regular, multiple, or irregular cycles with periods of 2–14 years, largely consistent across F to mid-M stars. Photometric amplitudes decrease with increasing rotation period, and comparisons across stellar ages show older, slowly rotating stars exhibit smooth cycles, while younger, rapidly rotating stars display abrupt variability. The transition occurs around 2–3 Gyr. Shorter baselines from *Kepler* detect activity modulations on 0.5–6 year timescales, suggesting correlations between rotation and cycle length, though short-term changes may arise from spot evolution and differential rotation. For M dwarfs, no clear dependence of cycle length on rotation has emerged, likely due to limited

baselines.

Asteroseismology provides complementary diagnostics, with activity-induced variations in oscillation frequency and amplitude correlating with stellar rotation, age, and activity. Chromospheric activity traced through Ca II H&K emission and the S-index has revealed cycles of a few years to several decades across hundreds of FGK stars, consistent with photometric trends and offering insight into solar analogs. Extending monitoring to M dwarfs shows larger cycle amplitudes, particularly in younger stars, while H $\alpha$  has also proven useful, often in conjunction with exoplanet surveys.

Coronal cycles detected in X-rays confirm chromospheric findings, despite observational challenges. Stars such as 61 Cyg A,  $\alpha$  Cen A and B, HD 81809,  $\iota$  Hor, and  $\epsilon$  Eri exhibit decade-long variability in coronal heating. Additional evidence for cycles comes from radio emission and flare statistics, which show polarity reversals and long-term variations.

Spectropolarimetric campaigns such as BCool directly probe large-scale field evolution via Zeeman-Doppler Imaging. These reveal polarity reversals and magnetic cycles across F—M stars with timescales from months to decades, sometimes consistent with chromospheric and coronal cycles but often showing complex evolution. Full cycles in M dwarfs remain elusive, though topology changes strongly suggest their presence.

In exoplanet research, stellar magnetic cycles introduce longterm radial velocity signals that may overshadow planetary signatures, primarily through magnetic inhibition of convective blueshift. Characterizing these signals is essential for reliable planet detection, while radial velocity data themselves provide an additional proxy for monitoring stellar cycles.

#### 3.2 General trends

The search for stellar activity cycles benefits from a multi-wavelength strategy, as different diagnostics probe dynamo action across distinct layers of stellar atmospheres and interiors. Photometric monitoring has proven to be the most productive approach, with detections numbering in the thousands and encompassing both short- and long-term cycles. Chromospheric monitoring through the S-index has yielded several hundred cycle detections, while asteroseismic studies have identified cycles in over a hundred stars. In contrast, only a handful of detections have been achieved through X-ray and spectropolarimetric observations. Importantly, spectropolarimetry provides direct sensitivity to magnetic (Hale-type) cycles, whereas other techniques predominantly reveal activity (Schwabe-type) cycles.

For the Sun, activity proxies from these methods display correlated temporal variations across the magnetic cycle. Brightness fluctuations track the evolution of chromospheric emission lines, S-index modulations, and soft X-ray variations. Acoustic oscillations also respond, with p-mode frequencies and amplitudes varying in phase and anti-phase with activity, respectively. Furthermore, the large-scale solar magnetic field shifts from a simple dipolar configuration at cycle minimum to a more complex topology at maximum, with enhanced quadrupolar components.

Analogous behaviour is observed in other stars. Younger, magnetically active stars tend to dim as their Ca II H&K emission increases, while older, less active stars brighten under the same conditions, mirroring the solar case. These patterns can be explained by the relative contributions of spots in young stars versus faculae in older stars. Cases of

synchronized photometric and chromospheric variations have been identified, as in HD 30495. For some stars, the large-scale magnetic topology evolves coherently with chromospheric activity, transitioning from simple dipolar states during minima to more complex multipolar structures during maxima, although correlations are not always straightforward. In certain cool dwarfs, only moderate or ambiguous relationships have been observed, reflecting the sensitivity of activity indices to both small- and large-scale magnetic features. More recently, anti-correlations between optical brightness and high-energy fluxes, such as those in Proxima Centauri, highlight diversity in stellar cycle behaviour compared with the Sun.

Trends emerging from long-term monitoring indicate that young, rapidly rotating stars often display irregular or chaotic variations, while older, slowly rotating stars exhibit smoother cycles with smaller amplitudes. Some stars display multiple cycles operating simultaneously on different timescales. Cycle morphologies, including asymmetric ascending and descending phases, bear similarities to the solar case, though the Sun remains particularly distinctive. As datasets expanded, empirical relationships between stellar rotation and cycle period emerged. Distinct scaling branches, traditionally labelled "active" and "inactive," were identified, with active stars hosting longer cycles at a given rotation period. These branches may reflect different dynamo mechanisms, potentially operating near the stellar surface in one case and near the base of the convection zone in the other. The Sun appears to lie between these branches, possibly occupying a transitional dynamo regime. A proposed framework suggests that activity cycles lengthen as stellar rotation slows with age, until a critical Rossby number is reached, after which magnetic braking weakens, the rotation rate stabilises, and cycles grow longer and weaker before disappearing entirely. However, more recent studies have challenged the universality of these branches, and the reality of such bifurcation remains debated.

#### References

- Acton L. Comparison of YOHKOH X-ray and other solar activity parameters for November 1991 to November 1995. In: Pallavicini R, Dupree AK, editors. Cool Stars, Stellar Systems, and the Sun. Vol. 109. Astronomical Society of the Pacific Conference Series; 1996. p. 45–52.
- Afram N, Berdyugina SV. Molecules as magnetic probes of starspots. Astron Astrophys. 2015;576:A34.
   Afram N, Berdyugina SV. Complexity of magnetic fields on red dwarfs. Astron Astrophys. 2019;629:A83.
- Alecian E, Wade GA, Catala C, Grunhut JH, Landstreet JD, Bagnulo S, Böhm T, Folsom CP, Marsden S, Waite I. A high-resolution spectropolarimetric survey of Herbig Ae/Be stars – I. Observations and measurements. Mon Not R Astron Soc. 2013;429(2):1001–1026.
- Alvarado-Gómez JD, Cohen O, Drake JJ, Fraschetti F, Poppenhaeger K, Garraffo C, Chebly J, Ilin E, Harbach L, Kochukhov O. Simulating the space weather in the AU Mic system: stellar winds and extreme coronal mass ejections. Astrophys J. 2022;928(2):147–163.
- 5. Amard L, Matt SP. The impact of metallicity on the evolution of the rotation and magnetic activity of Sunlike stars. Astrophys J. 2020;889(2):108–118.
- 6. Anderson RI, Reiners A, Solanki SK. On detectability of Zeeman broadening in optical spectra of F- and G-dwarfs. Astron Astrophys. 2010;522:A81.
- 7. Andretta V, Busà I, Gomez MT, Terranegra L. The Ca II

- infrared triplet as a stellar activity diagnostic. I. Non-LTE photospheric profiles and definition of the RIRT indicator. Astron Astrophys. 2005;430:669–677.
- 8. Aurière M, Konstantinova-Antova R, Charbonnel C, Wade GA, Tsvetkova S, Petit P, Dintrans B, Drake NA, Decressin T, Lagarde N, Donati JF, Roudier T, Lignières F, Schröder KP, Landstreet JD, Lèbre A, Weiss WW, Zahn JP. The magnetic fields at the surface of active single G–K giants. Astron Astrophys. 2015;574:A90.
- 9. Aurière M, Wade GA, Konstantinova-Antova R, Charbonnel C, Catala C, Weiss WW, Roudier T, Petit P, Donati JF, Alecian E, Cabanac R, van Eck S, Folsom CP, Power J. Discovery of a weak magnetic field in the photosphere of the single giant Pollux. Astron Astrophys. 2009;504(1):231–237.
- Ayres TR. In the trenches of the solar-stellar connection.
  Ultraviolet and X-ray flux-flux correlations across the activity cycles of the Sun and Alpha Centauri AB. Astrophys J Suppl Ser. 2020;250(1):16–29.
- 11. Babcock HW. Magnetic intensification of stellar absorption lines. Astrophys J. 1949;110:126–134.
- 12. Babcock HW. The topology of the Sun's magnetic field and the 22-year cycle. Astrophys J. 1961;133:572–587. Babcock HW, Babcock HD. The Sun's magnetic field, 1952–1954. Astrophys J. 1955;121:349–359.
- 13. Bai T. Periodicities in solar flare occurrence: analysis of cycles 19–23. Astrophys J. 2003;591(1):406–415.
- 14. Baliunas SL, Donahue RA, Soon WH, Horne JH, Frazer J, Woodard-Eklund L, Bradford M, Rao LM, Wilson OC, Zhang Q, Bennett W, Briggs J, Carroll SM, Duncan DK, Figueroa D, Lanning HH, Misch T, Mueller J, Noyes RW, Poppe D, Porter AC, Robinson CR, Russell J, Shelton JC, Soyumer T, Vaughan AH, Whitney JH. Chromospheric variations in main-sequence stars. II. Astrophys J. 1995;438:269–287.
- Baliunas SL, Horne JH, Porter A, Duncan DK, Frazer J, Lanning H, Misch A, Mueller J, Noyes RW, Soyumer D, Vaughan AH, Woodard L. Time-series measurements of chromospheric Ca II H and K emission in cool stars and the search for differential rotation. Astrophys J. 1985;294:310–325.
- 16. Baliunas SL, Vaughan AH. Stellar activity cycles. Annu Rev Astron Astrophys. 1985;23:379–412.
- 17. Basri G, Marcy GW. Zeeman enhancement of lines in extremely active K dwarfs. Astrophys J. 1994;431:844–853
- 18. Basri G, Marcy GW, Valenti JA. Limits on the magnetic flux of pre-main-sequence stars. Astrophys J. 1992;390:622–632.
- 19. Basri G, Shah R. The information content in analytic spot models of broadband precision light curves. II. Spot distributions and lifetimes and global and differential rotation. Astrophys J. 2020;901(1):14–27.
- Basri G, Walkowicz LM, Batalha N, Gilliland RL, Jenkins J, Borucki WJ, Koch D, Caldwell D, Dupree AK, Latham DW, Meibom S, Howell S, Brown T. Photometric variability in Kepler target stars: the Sun among stars—a first look. Astrophys J. 2010;713(2):L155–L159.
- 21. Basri G, Walkowicz LM, Reiners A. Comparison of Kepler photometric variability with the Sun on different timescales. Astrophys J. 2013;769(1):37–48.
- 22. Basu S. Global seismology of the Sun. Living Rev Sol Phys. 2016;13(1):2–24.
- 23. Baum AC, Wright JT, Luhn JK, Isaacson H. Five decades

- of chromospheric activity in 59 Sun-like stars and new Maunder minimum candidate HD 166620. Astron J. 2022;163(4):183–195.
- 24. Bellotti S, Evensberget D, Vidotto AA, Lavail A, Lüftinger T, Hussain GAJ, Morin J, Petit P, Boro Saikia S, Danielski C, Micela G. Spectropolarimetric characterisation of exoplanet host stars in preparation of the Ariel mission: magnetic environment of HD 63433. Astron Astrophys. 2024;688:A63.
- 25. Bellotti S, Fares R, Vidotto AA, Morin J, Petit P, Hussain GAJ, Bourrier V, Donati JF, Moutou C, Hébrard EM. The space weather around the exoplanet GJ 436b. I. The large-scale stellar magnetic field. Astron Astrophys. 2023;676:A139.
- 26. Bellotti S, Morin J, Lehmann LT, Folsom CP, Hussain GAJ, Petit P, Donati JF, Lavail A, Carmona A, Martioli E, Romano Zaire B, Alecian E, Moutou C, Fouqué P, Alencar S, Artigau E, Boisse I, Bouchy F, Cadieux C, Cloutier R, Cook N, Delfosse X, Doyon R, Hébrard G, Kochukhov O, Wade G. Monitoring the large-scale magnetic field of AD Leo with SPIRou, ESPaDOnS and Narval: toward a magnetic polarity reversal? arXiv e-prints. 2023;arXiv:2307.01016.
- 27. Bellotti S, Morin J, Lehmann LT, Petit P, Hussain GAJ, Donati JF, Folsom CP, Carmona A, Martioli E, Klein B, Fouqué P, Moutou C, Alencar S, Artigau E, Boisse I, Bouchy F, Bouvier J, Cook NJ, Delfosse X, Doyon R, Hébrard G. Long-term monitoring of large-scale magnetic fields across optical and near-infrared domains with ESPaDOnS, Narval and SPIRou: the cases of EV Lac, DS Leo, and CN Leo. arXiv e-prints. 2024;arXiv:2403.08590.
- 28. Sanchez S, Fournier A, Jouve L, Brun AS. The solar dynamo: from observations to numerical simulations. Astron Astrophys. 2014;563:A113.
- Saar SH. Recent measurements of stellar magnetic fields. In: Stenflo JO, editor. Solar and Stellar Magnetic Fields: Origins and Coronal Effects. IAU Symposium No. 130. Dordrecht: Reidel; 1988. p. 431–445.
- 30. Reiners A. Observations of cool-star magnetic fields. Living Rev Sol Phys. 2012;9(1):1–75.
- 31. Muirhead PS, Veyette MJ, Mace GN, Mann AW, Rojas-Ayala B, Thorp R, Riedel AR, Newton ER, Covey KR, Cruz KL, Terrien RC. Diagnosing magnetic fields in M dwarfs using curve-of-growth diagrams. Astron J. 2020;160(3):159–176.
- 32. Johns-Krull CM, Valenti JA, Koresko C. Measuring the magnetic fields of T Tauri stars. Astrophys J. 1999;516(2):900–915.
- 33. Shulyak D, Reiners A, Seemann U, Kochukhov O, Piskunov N. The magnetic field and activity of the very active M dwarf YZ CMi. Astron Astrophys. 2014;563:A35.
- 34. Donati JF, Semel M, Carter BD, Rees DE, Cameron AC. Spectropolarimetric observations of active stars. Mon Not R Astron Soc. 1997;291(4):658–682.